IPP/CNRS-A017: A chemical probe for human dihydroorotate dehydrogenase (hDHODH)

Andreas Krämer, Amelie Tjaden, Benardina Ndreshkjana, Claudia Tredup, Henner Farin, Stefan Knapp, Yves Janin, Susanne Müller

Current Research in Chemical Biology 2 (2022) 100034

Contents lists available at ScienceDirect

Current Research in Chemical Biology

journal homepage: www.journals.elsevier.com/current-research-in-chemical-biology

IPP/CNRS-A017: A chemical probe for human dihydroorotate dehydrogenase (hDHODH)*

Andreas Krämer [a,b,d,**], Amelie Tjaden [a,b], Benardina Ndreshkjana [c,d], Claudia Tredup [a,b], Henner F. Farin [c,d,e], Stefan Knapp [a,b,d], Yves L. Janin [f], Susanne Müller [a,b,*]

[a] Institute of Pharmaceutical Chemistry, Johann Wolfgang Goethe University, Max-von-Laue-Str. 9, 60438, Frankfurt am Main, Germany
[b] Buchmann Institute for Molecular Life Sciences and Structural Genomics Consortium (SGC), Max-von-Laue-Str. 15, 60438, Frankfurt am Main, Germany
[c] Georg-Speyer-Haus, Institute for Tumor Biology and Experimental Therapy, Frankfurt am Main, Germany
[d] Frankfurt Cancer Institute, Goethe University, Frankfurt am Main, Germany
[e] German Cancer Consortium (DKTK), Heidelberg, Germany
[f] Structure et Instabilité des Génomes (StrInG), Muséum National d'Histoire Naturelle, INSERM, CNRS, Alliance Sorbonne Université, 75005 Paris, France

ARTICLE INFO

Keywords:
hDHODH
Crystal structure
Chemical probe
Organoids
Viability assessment

ABSTRACT

Human Dihydroorotate dehydrogenase, which catalyses *de novo* pyrimidine biosynthesis, is an emerging target for treatment of infectious diseases, arthritis and cancer. In order to provide a chemical tool studying this key enzyme, we characterized IPP/CNRS-A017, a highly potent, selective, and cell-active inhibitor of the human Dihydroorotate dehydrogenase (hDHODH). In this report, we describe the crystal structure of IPP/CNRS-A017 in complex with hDHODH, providing inside into its binding mode. Additionally, further off-target profiling in a kinome-wide screen and a G-Protein-Coupled Receptors screen as well as investigated cell viability effects in three different cell lines (HEK293T, U2OS, human fibroblasts) confirmed that IPP/CNRS-A017 is a highly selective chemical tool to study the biology of hDHODH. Specific sensitivity to IPP/CNRS-A017 was observed in patient-derived colorectal cancer organoids.

1. Introduction

Human Dihydroorotate dehydrogenase catalyses the fourth step of the *de novo* pyrimidine biosynthesis. The enzyme is located on the outer surface of the inner mitochondrial membrane (IMM), while all other proteins involved in this pathway are cytosolic (Munier-Lehmann et al., 2013). The enzyme converts dihydroorotate to orotate. DHODH uses Flavin mononucleotide (FMN) as a co-factor, which takes the electrons and passes them on to reduce ubiquinone to ubiquinol, thus reconstituting the cofactor (Fig. 1A). Known ligands of this enzyme are thought to block the ubiquinone binding site ending the reaction cycle. Several inhibitors are currently under investigation for the treatment of various diseases, ranging from viral and parasitic infections to autoimmune disease (Munier-Lehmann et al., 2013; Reis et al., 2017; Boschi et al., 2019) (Fig. 1B). Clinical trials led to approval of leflunomide (ARAVA; 5-methyl-*N*-[4-(trifluoromethyl) phenyl]-isoxazole-4-carboxamide) as a disease-modifying antirheumatic drug for the treatment of rheumatoid arthritis and psoriatic arthritis (van Riel et al., 2004). However, leflunomide functions as a pro-drug that yields the metabolite teriflunomide, inhibiting DHODH with modest activity (0.6 μM) (Fox et al., 1999). Other clinically investigated inhibitors include the 4-quinolinecarboxylic acid derivative Brequinar (DuP-785), which exhibits only a narrow therapeutic window in clinical

Abbreviations: HEPES, 2-[4-(2-hydroxyethyl)piperazin-1-yl]ethanesulfonic acid; FMN, Flavin mononucleotide; RMSD, root-mean-square deviation; PDB, Protein Data Bank; PDTO, patient-derived tumor organoid; ORO, orotate; TCEP, Tris(2-carboxyethyl)phosphine; hDHODH, human Dihydroorotate Dehydrogenase; LDAO, N,N-Dimethyldodecylamine N-oxide; EDTA, Ethylenediaminetetraacetic acid; GST, Glutathione S-transferase; TEV, Tobacco Etch Virus; PEG, Polyethylene glycol; TRIS, tris(hydroxymethyl)aminomethan; AML, Acute myeloid leukemia; DLBCL, diffuse large B-cell lymphoma; SGC, Structural Genomics Consortium; UMPS, Uridine monophosphate synthase; PRPP, Phosphoribosyl pyrophosphate.

* Professor Stefan Knapp, the coauthor author on this paper is the Editor-in-Chief of this journal, but this author had no involvement in the peer review process used to assess this work submitted to Current Research in Chemical Biology. This paper was assessed and the corresponding peer review managed by Professor Dan Yang a member of the Advisory Board.

* Corresponding author. Institute of Pharmaceutical Chemistry, Johann Wolfgang Goethe University, Max-von-Laue-Str. 9, 60438, Frankfurt am Main, Germany.
** Corresponding author.Institute of Pharmaceutical Chemistry, Johann Wolfgang Goethe University, Max-von-Laue-Str. 9, 60438, Frankfurt am Main, Germany.
E-mail addresses: kraemer@pharmchem.uni-frankfurt.de (A. Krämer), susanne.mueller-knapp@bmls.de (S. Müller).

https://doi.org/10.1016/j.crchbi.2022.100034
Received 24 January 2022; Received in revised form 3 May 2022; Accepted 6 June 2022

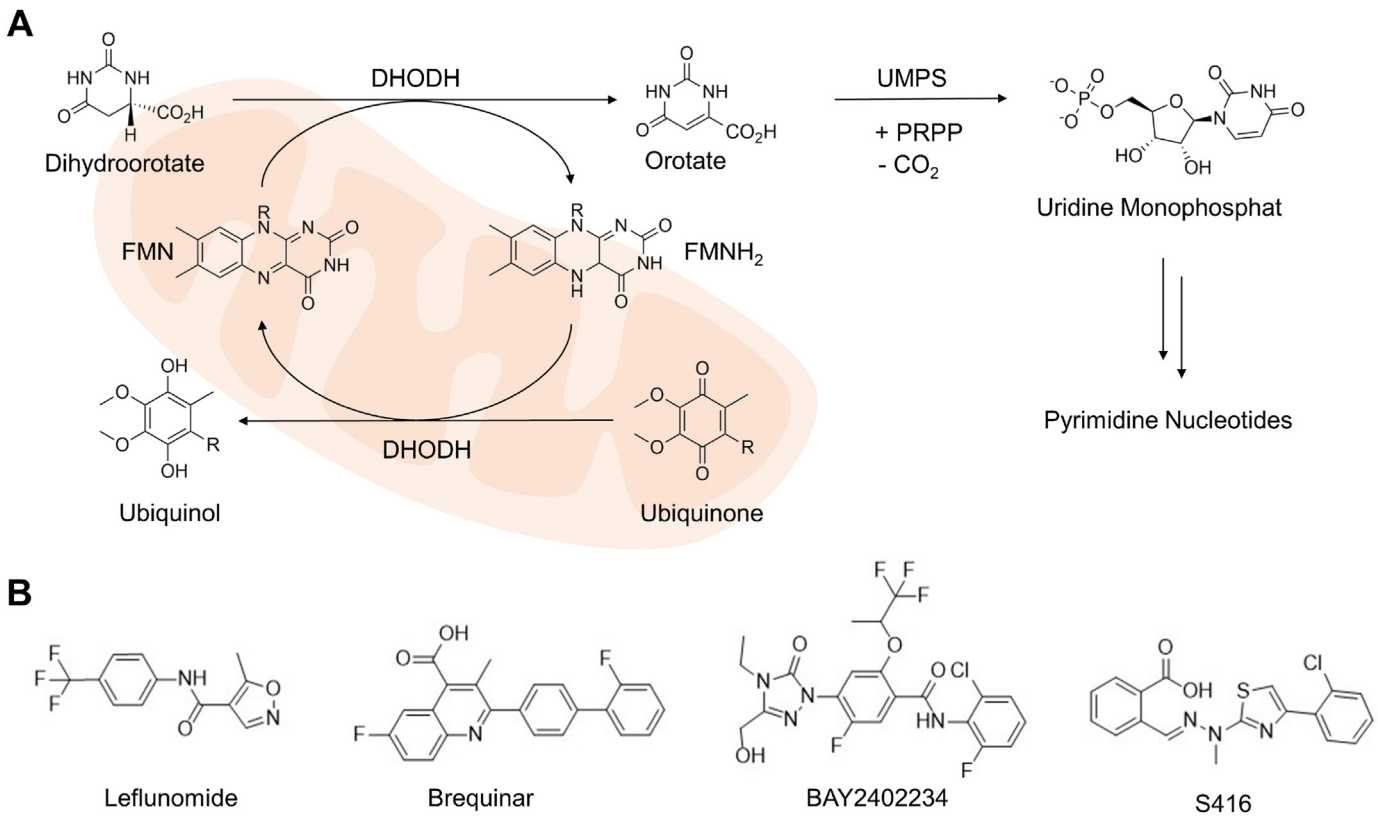

Fig. 1. A: Conversion of dihydroorotate to orotate by DHODH during Pyrimidine biosynthesis. Abbreviations: DHODH (Dihydroorotate dehydrogenase); UMPS (Uridine monophosphate synthase); FMN (Flavin mononucleotide); PRPP (Phosphoribosyl pyrophosphate) **B:** Selected chemical structures of DHODH inhibitors.

trials evaluating this inhibitor as immunosuppressant (Vyas and Ghate, 2011), as well as the methylhydrazinylidene S416 (GTPL-11164), which has been investigated as an antiviral agent (Xiong et al., 2020). Recently, DHODH has gained attention as a possible target in acute myeloid leukemia (AML) (Christian et al., 2019; Sykes, 2018) as the growth of cancer cells might be metabolically dependent on the *de novo* pyrimidine biosynthesis, opening a new avenue for therapeutic intervention (Sykes, 2018). Initial trials showed promising results, indicating that DHODH inhibitors have both cytotoxic as well as pro-differentiation activity in AML (Christian et al., 2019; Sykes et al., 2016; Madak et al., 2019).

Chemical probes are potent, selective small-molecule tools that have been comprehensively characterized, enabling studies of specific protein targets within complex biological systems. In contrast to many drugs, chemical probes are highly selective within their target family and ideally, they have been characterized against other major target families that often contribute to off-target effects when unintentionally inhibited. To reduce the risk of undiscovered off-target effects, it is recommended that a negative control compound is provided that should be highly structurally related to the chemical probe but inactive against the target (Drewes and Knapp, 2018). The described inhibitor, together with its matched negative control compound fulfil the criteria of a chemical probe and are available via the Donated Chemical Probes Program (https://opensciencesprobes.sgc-frankfurt.de/) (M ü ller et al., 2018; Arrowsmith et al., 2015).

Given the current interest in hDHODH as an important drug target in several diseases, there is a clear need for a chemical probe to study cellular process. Several compounds are available, but none fulfil the stringent probe criteria (M ü ller et al., 2018) (Table 1). The FDA approved drug Leflunomide for instance is only a weak inhibitor of DHODH and has off-target activity on tyrosine kinases and NF-κB signalling (Breedveld and Dayer, 2000). For two other compounds, Brequinar already developed in the 1980s and the recently disclosed BAY2402234 (Orludodstat) (Christian et al., 2019) a negative control is missing and no comprehensive off-target profile has been published (Peters, 2018), making it difficult to interpret data obtained using these chemical tool compounds, especially in cellular phentotypic experiments.

In this report, we present the chemical probe for the human DHODH, **IPP/CNRS-A017,** and its matched inactive control compound, **IPP/CNRS-A019**. We provide the crystal structure along with biophysical characterisations and screening outside its target family to exclude off-target activity. Taken together, our characterization data reveal that **IPP/CNRS-A017** is a useful tool to study hDHODH.

Table 1
Analysis of hDHODH probe set.

Probe criteria	Results /Evaluation
Inhibitor/agonist potency (goal is < 100 nM (IC_{50} or K_D))	IC_{50} of 25 nM in activity assay)[a] K_D = 79 nM ± 40 (ITC)
Selectivity within target family: >30-fold	not applicable
Selectivity outside target family: Off-targets	Met: GPCR screen (44 targets) PBR K_D = 2.1 μM Alph1D K_D = 4.1 μM Sigma 2 K_D = 583 nM No activity in Eurofins KINOMEscan®
On target cell activity for cell-based targets: (goal is < 1 μM IC_{50}/EC_{50})	EC_{50} = 2.5 nM (HEK293 measles assay)
Negative control (goal is *in vitro* potency >100 times less; Cell activity (goal is > 100 times less potent than the probe)	IC_{50} = 1.2 μM (measles assay); 480-fold[a] IPP/CNRS-A019 (negative control (inactive at 10 μM)

[a] Data taken from Lucas-Hourani et al. (2015) and Munier-Lehmann et al. (2015). Complete Data of KINOMEscan® and GPRCR scan can be found in Supplement Information Tables S2 and S3.

2. Material and methods

2.1. Expression of hDHODH

The N-terminally truncated hDHODH (aa31-396) construct was expressed in *E. coli* Rosetta cells using a pFN2A vector (kind gift from M. Lolli University of Turin, Italy). The protein was N-terminally fused to a GST-tag and TEV-cleavage site. Cultures were grown at 37 °C in 2 × TY media (Roth) supplemented with 0.1 mM flavin mononucleotide (Fisher Scientific) and 50 mg/mL ampicillin (Roth). Expression was induced at an OD600 with 0.5 mM IPTG (Zellbio) and the cultures were further incubated at 16 °C for 18 h, before harvesting (6000×*g*, 10 min).

2.2. Purification of hDHODH

Cells were resuspended in lysis buffer (50 mM HEPES (Fisher Scientific), pH 7.5, 400 mM NaCl (Fisher Scientific), 10% Glycerol (Fisher Scientific), 1 mM TCEP (Zellbio), 0.33% Thesit (Merck) and disrupted by sonication. After centrifugation (20.000×*g*, 20 min), the supernatant containing the GST-tag fused enzyme was loaded onto in a drop column filled with 5 mL immobilized glutathione-sepharose beads (GE Healthcare), and washed with 100 ml lysis buffer. The GST-Tag was cleaved by adding the TEV protease directly to the column along with 5 mL of lysis buffer. The closed column was slowly rotated overnight. Next day the flow through was collected, and the column was washed with more lysis buffer until the elution was colourless (hDHODH has an orange colour). The protein containing fractions were pooled together, concentrated to approx. 4–5 mL, and loaded onto Superdex 75 16/60 HiLoad gel filtration column (GE Healthcare) equilibrated with final buffer (25 mM Tris pH 7.5, 400 mM NaCl, 1 mM EDTA, 10% Glycerol, 2 mM TCEP, 0.05% Thesit). The protein was eluted with a flow rate of 1 mL/min, concentrated to 20 mg/mL and directly used for crystallization.

2.3. Crystallization of hDHODH

DHODH (20 mg/mL) was mixed with 2 mM orotate (Fisher Scientific), 1 mM IPP/CNRS-A017, 20.8 mM LDAO (Alfa Aesar) and incubated for 1 h. This solution was mixed in a 1:1 ratio with the reservoir solution containing 26–33% PEG400 (Molecular Dimensions), 0.2 M KSCN (Fisher Scientific) 0.2 M NaBr (Fisher Scientific), and 0.1 M acetate pH 4.8 (Fisher Scientific). Orange cubic like crystals appeared after 8–12 days at 20 °C.

2.4. Data collection and refinement

Diffraction data were collected at beamline X06SA (SLS, Villigen, CH) at a wavelength of 1.0 Å at 100 K. Data were integrated using XDS (Kabsch and XDS, 2010) and scaled with aimless (Evans and Murshudov, 2013). The PDB structure with the accession code 5MVC (Sainas et al., 2017) was used as an initial search MR model using the program MOLREP (Lebedev et al., 2008). The final model was built manually using Coot (Emsley and Cowtan, 2004) with iterative refinement steps of REFMAC5 (Vagin et al., 2004). Data collection and refinement statistics are summarized in Table S1. The structure has been deposited in the PDB under accession code 6SYP.

2.5. Viability assessment

Viability of three different cell lines was tested using a live cell high-content screen as described previously (Howarth et al., 2020; Heitel et al., 2020; Tjaden et al., 2022). In brief HEK293T (ATCC® CRL-1573™) and U2OS (ATCC®HTB-96™) were cultured in DMEM plus L-Glutamine (High glucose) supplemented by 10 % FBS (Gibco) and Penicillin/Streptomycin (Gibco). MRC-9 fibroblasts (ATCC® CCL-2™) were cultured in EMEM plus L-Glutamine supplemented by 10 % FBS (Gibco) and Penicillin/Streptomycin (Gibco). For every cell line 2000 cells per well were seeded in 384 well plates in culture medium (Cell culture microplate, PS, f-bottom, μClear®, 781091, Greiner). Cells were stained with 60 nM Hoechst33342 (Thermo Scientific), 75 nM Mitotracker red (Invitrogen), 0.3 μl/well Annexin V Alexa Fluor 680 conjugate (Invitrogen) and 25 nL /well BioTracker™ 488 Green Microtubule Cytoskeleton Dye (EMD Millipore). Each compound (IPP/CNR-A019, IPP/CNR-A017) was tested at two different concentrations (1 μM and 10 μM) in triplicates. Staurosporine at 10 μM was used as a positive control. Fluorescence and cellular shape measured before compound treatment, 12 h and 24 h after compound exposure, respectively using the CQ1 high-content confocal microscope (Yokogawa). The following setup parameters were used for image acquisition: Ex 405 nm/Em 447/60 nm, 500 ms, 50%; Ex 561 nm/Em 617/73 nm, 100 ms, 40%; Ex 488/Em 525/50 nm, 50 ms, 40%; bright field, 300 ms, 100% transmission, one centered field per well, 7 z stacks per well with 55 μm spacing. Images were analysed using the CellPathfinder software (Yokogawa). Cells were detected as described previously (Howarth et al., 2020), gated using a machine learning algorithm and divided in the categories healthy, apoptotic, lysed and dead cells. Data was normalized against the average of DMSO (0.1%) treated cells.

To assess the viability of U2OS cells in presence or absence of uridine (10 μg/ml and 20 μg/ml, Roth), a simple confluence assay was performed over 78 h. U2OS cells (ATCC®HTB-96™) were cultured in DMEM plus L-Glutamine (High glucose) supplemented by 10 % FBS (Gibco) and Penicillin/Streptomycin (Gibco). One day prior to compound exposure, 1250 cells per well were seeded in 384 well plates in culture medium (Cell culture microplate, PS, f-bottom, μClear®, 781091, Greiner). The enhanced contour was measured before and every 6 h after compound treatment (IPP/CNR-A019, IPP/CNR-A017) over 78 h using the Cellcyte X (Cytena) microscope. The compounds were tested in a 6-fold dilution (0,5 μM, 1 μM, 2 μM, 5 μM, 10 μM). Confluence was analysed using the implemented Cellcyte software. Error bars show SEM of four technical replicates. Two biological replicates were performed.

2.6. Patient-derived organoids culture and drug testing

Resection samples from colorectal cancer patients were provided by the University Cancer Center Frankfurt (UCT). All materials were collected after prior written informed consent as part of the interdisciplinary Biobank and Database Frankfurt (iBDF) and the study was approved by the institutional review board of the University Hospital Frankfurt (#274-18). Patient-derived organoids were established and maintained as described previously (van de Wetering et al., 2015). Organoid medium contained advanced DMEM/F12 supplemented with 10 mM HEPES, 1 × Glutamax, 1 × penicillin/streptomycin, 2% B27, 12.5 mM N-acetylcysteine, 500 nM A83-01 (R&D Systems), 10 μM SB202190 (Sigma-Aldrich), 20% R-spondin 1 conditioned medium, 10% Noggin conditioned medium, 50 ng/ml human EGF (Peprotech). 10 μM of Y-27632 was added to the medium for the first 3 d after seeding or passaging. Organoids were enzymatically dissociated with Accutase (Thermo Fischer), and single cells were filtered (40 μm, 542040, Greiner) and counted after trypan blue staining. Cells were seeded in 15 μl Matrigel in 96-well round bottom plates (Sarstedt) and overlaid with 100 μl organoid medium per well that additionally contained 100 μg/ml Primocin (InvivoGen) and 35 ng/ml Wnt surrogate (U-Protein Express). For each line, an adjusted cell number was seeded to obtain 300 organoids per well as determined prior by colony forming assay. Plates were sealed with Breath-easy membranes (Sigma Aldrich) and after 3 days the medium was changed, and drugs were added using a D300e digital dispenser (Tecan). Cells were exposed to a 7-point drug dilution (0.01–10 μM) of A017 and A019 (each at 10 mM stock concentration in DMSO) in the presence or absence of 10 μg/ml uridine (Roth). The total volume of DMSO was kept constant. After 4 days of treatment, morphological images were captured (EVOS Fl, Life Technologies) and

cell viability was assessed using CellTiter-Glo assay (Promega) following the manufacturer's recommendations. Luminescence was measured on a SpectraMax iD3 Microplate Reader (Molecular Devices). Average results from triplicate wells were measured and dose-response curves were generated in Prism 9.2.0 (GraphPad Inc).

2.7. Isothermal titration calorimetry

For ITC measurements, hDHODH was diluted with SEC buffer to the desired concentration (final conc. 25 μM). The probe and its negative control were diluted from a 10 mM DMSO (Roth) stock in the same buffer (final conc. 150 μM). The DMSO concentration in the protein solution was adjusted accordingly. ITC measurements were performed using an Affinity ITC (TA-Instruments) at a temperature of 25 °C and a stirring rate of 75 rpm. The probe was titrated into the protein solution (172 μL cell volume) with 2.5 μL per injection, except the first injection which was 1 μL. The time between each injection was set to 300 s. The results were analysed using the NanoAnalyze Software (TA instruments). The curve can be found in the supplement (Fig. S2).

3. Results and discussion

3.1. IPP/CNRS-A017 a chemical probe

The discovery of IPP/CNRS-A019 originated from a chemistry-oriented approach focusing on the generation of a series of original chemical entities featuring an alkoxypyrazole component. Screening of these libraries, using a bioluminescence-based measles replication assay, led to the identification of two hits. From these, the reported iterations of design, synthesis and evaluations not only provided optimized inhibitors such as IPP/CNRS-A017 but also led to the identification of hDHODH as the cellular target accounting for this antiviral effect (Lucas-Hourani et al., 2015; Munier-Lehmann et al., 2015). Further systematic analysis and evaluation with specific assays and protein selectivity panels identified IPP/CNRS-A017 and its matched inactive control IPP/CNR-A019 (Lucas-Hourani et al., 2015) (Fig. 2) as a suitable chemical tool set, which fulfils or surpasses the predefined probe criteria (see Table 1). To determine the *in cellulo* and *in vitro* potency, previously a measles virus inhibition assay as well as an activity assay-based monitoring the reduction of DCIP were used, respectively (Lucas-Hourani et al., 2015; Munier-Lehmann et al., 2015). A selective screen within the target family was not possible, since hDHODH is the only member of this enzyme family in human. In order to determine activity outside the target family,

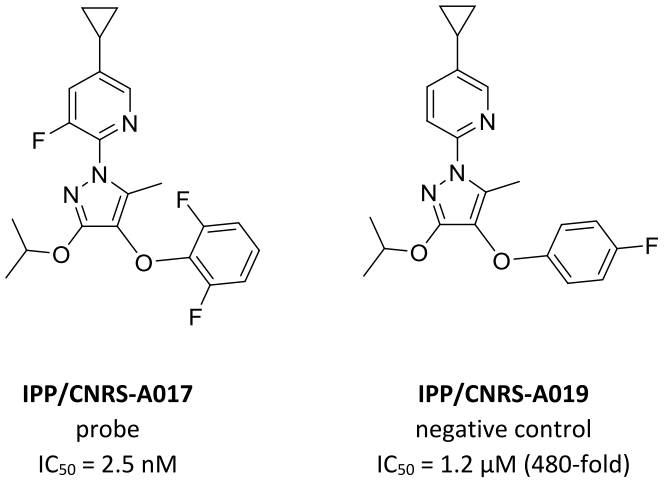

Fig. 2. Chemical structures of the hDHODH chemical probe set with inhibition data from measles virus assay (Lucas-Hourani et al., 2015).

PDSP GPCR Scan of 45 GPCRs was performed at 10 μM at the National Institute of Mental Health (NIMH) Psychoactive Drug Screening Program (https://pdspdb.unc.edu/pdspWeb/), followed up with the determination of the Ki for targets with >50 % inhibition (Besnard et al., 2012). Within the GPCR family, selectivity screening data revealed only minor off-target activity on PBR, Sigma 2 and Alph1D of with Ki of 2.1 μM, 4.1 μM and 0.6 μM, respectively. However, there is a sufficient window compared to hDHODH of at least 25-fold or more.

A recent study showed that the RAF kinase inhibitor TAK-632 exhibits hDHODH activity (Abt et al., 2019). To exclude potential kinase activity for IPP/CNRS-A017, kinase selectivity of the probe and inactive control was assessed in a comprehensive kinase panel of 468 kinases (KINOMEscan® DiscoverX, Eurofins). Pleasingly, no off-target activity was detected at screening concentrations of 1 μM. All probe criteria and activity data are summarized in Table 1.

3.2. Crystal structure

To gain insight into the binding mode that may explain the potency and selectivity of the developed chemical probe, the co-crystal structure was determined and refined at a resolution of 1.8 Å. Human DHODH crystallized in the space group $P3_221$. Electron density was observed for 347 of the 365 residues primary structure. In addition, electron density was observed for the reaction product orotate (ORO), the co-factor flavin mononucleotide (FMN) and the probe IPP/CNRS-A017 (Fig. 3). The protein adopted the same overall folding as observed in other published hDHODH structures (Christian et al., 2019; Sainas et al., 2017; Baumgartner et al., 2006). The structure consisted of a large C-terminal domain (Met78-Arg396) with a central α/β-barrel and a small N-terminal domain (Met30-Leu68). The N-terminal domain comprised of two mainly hydrophobic alpha helices (α1 and α2) which were attached to the mitochondrial intermembrane in cells. In the determined structure, the electron density for the α1 helix was poorly resolved. In the transition area between the membrane and the soluble part of the protein a tunnel to the active site was formed (Fig. 3C). The highly hydrophobic entrance of the tunnel has been suggested to be the ubiquinone binding site (Rawls et al., 2000). IPP/CNRS-A017 occupied this cavity completely (Fig. 3B) thereby preventing ubiquinone from binding, explaining the mode of action of the developed chemical tool. Strikingly, the compound seemed to be only attracted and kept in position by hydrophobic interactions, as no obvious hydrogen bonds were found. The ligand made extensive non-polar interactions with surrounding residues Pro53, Ala55, His56, Leu58, Ala59, Phe62, Thr63, Leu67, Leu68, Pro69, Phe98, Val134, Leu359, Tyr356, Thr360 and Pro364 (Fig. 3A). In order to understand the high potency of this compound in the absence of hydrogen bonds, we compared our structure with the recently published complex of BAY 20402234 (Fig. 3D) and a Leflunomide analogue (Fig. 3E). Even though these molecules are based on entirely different chemical scaffolds, the occupied space inside the binding pocket was almost identical (Christian et al., 2019; Lucas-Hourani et al., 2015). This is specifically illustrated by comparing IPP/CNRS-A017 with the leflunomide derivative where both isopropyl moieties at the top and aryl moieties at the bottom of the binding pocket were perfectly aligned. Thus, strong inhibitors of DHODH can be designed based on highly diverse scaffolds. As a common feature all inhibitors were mainly hydrophobic molecules with two to three aromatic ring-systems which perfectly filled in the binding crevice.

Remarkably, significant loss of activities is observed when shifting from IPP/CNRS-A017 to IPP/CNRS-A019. It is noteworthy and not straightforward to account for. Indeed, as observed in the crystal structure, a change from the fluorine atoms on both ortho position to a single fluorine on the para position of the same ring was not expected to lead to any significant steric changes capable of accounting for this difference. A more plausible explanation lies in the angle value between the fluorinated aromatic and the alkoxypyrazole ring. We suggest, that the two fluorine atoms of IPP/CNRS-A017 are inducing a change of this angle due to their proximity with the oxygen linking these two rings. This small

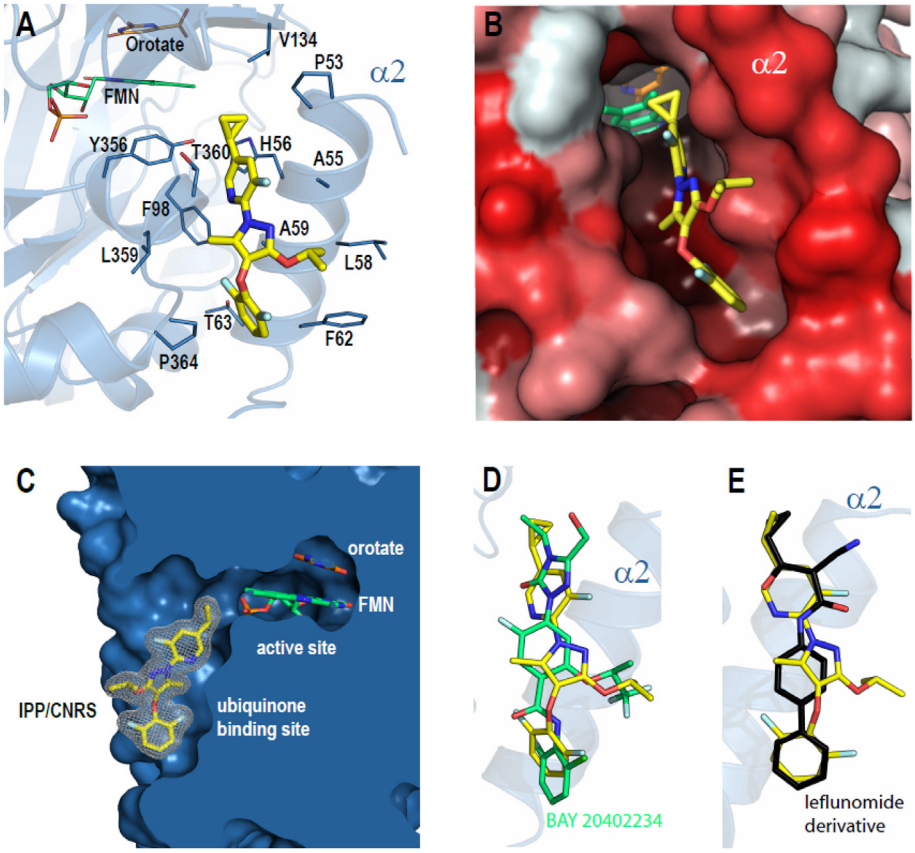

Fig. 3. Crystal structure of IPP/CNRS-A017 bound to hDHODH.
A: Binding of IPP/CNRS-A017 to hDHODH in cartoon-stick representation. The ligand is depicted in yellow, FMN in green and orotate in orange. Additionally, the surrounding, mainly nonpolar residues are indicated. **B:** Hydrophobic surface of the binding pocket; red refers to hydrophobic and white to none-hydrophobic residues, respectively. The ligand is attracted by hydrophobic forces alone. **C:** Surface slice of the binding pocket and the active site. The ubiquinone binding site is connected via a small tunnel to the active site. Additionally, the electron density map of the IPP/CNRS-A017 is shown as a $2F_o$-F_c-map contoured at 1.5 σ. The colour scheme is identical to A. **D:** Overlay of IPP/CNRS-A017 and BAY 20402234 (PDB 6QU7) and **E:** with a leflunomide derivative (PDB 3G0X). Despite different scaffolds the binding inside the pocket is remarkably similar. . (For interpretation of the references to color in this figure legend, the reader is referred to the Web version of this article.)

change of the angle would translate into a deviation in thermodynamic cost for the inhibitors to fit within the ubiquinone binding site of DHODH and thus explain why many biarylether analogues lacking such angle-constraining substituents, including the para fluoro-bearing analogue IPP/CNRS-A019, are much less active (Lucas-Hourani et al., 2015; Munier-Lehmann et al., 2015).

3.3. Viability assessment

For mechanistic studies, the toxicity profile of chemical probes needs to be known to exclude non-specific effects on signalling and metabolism. To determine the dose- and time-dependent influence of IPP/CNRS-A017 (A017) and its negative control IPP/CNR-A019 (A019) on cell viability, a live cell high content screen was performed in three different cell types: human embryonic kidney cells (HEK293T), osteosarcoma cells (U2OS), and non-transformed human lung fibroblasts (MRC-9) (Tjaden et al., 2022). After 24 h of compound treatment, neither the IPP/CNR probe compound A017 nor its negative control (A019) showed significant toxic effects at both tested concentrations (10 μM and 1 μM) in all tested cell lines (Fig. 4A). The apoptotic rate after 24 h of treatment with the probe compound A017 was slightly increased at 10 μM in comparison to the negative control, (Fig. 4B, Fig. S1). No difference was observed at a concentration of 1 μM of compound treatment compared to the DMSO 0.1 % treated cells. In addition, the compounds had no major effect on microtubule or cellular shape (Fig. 4C, Fig. S1). None of the compounds showed precipitation or increased levels of cell lysis.

To test whether the effect of DHODH inhibition can be overcome through the addition of uridine, the final product of the pyrimidine pathway (Fig. 1), we performed a uridine rescue experiment (Fig. 5). U2OS cells were incubated in presence or absence of uridine (10 μg/ml and 20 μg/ml) for 72 h and confluence was recorded (Christian et al., 2019; Sykes et al., 2016).

Already after 48 h, reduced confluence was observed in the presence of the probe compound (A017), an effect that was even more pronounced after 72 h (Fig. 5A). This effect was not observed after the treatment with the inactive control compound (A019). The effect of the probe compound could be rescued by the addition of uridine, bypassing the need for DHODH activity.

The probe compound had an effect of more than 50% on cell confluence after 72 h at all tested concentrations (Fig. 5B). As expected, addition of uridine at either concentration (10 μg/mL or 20 μg/mL) lead to a rescue effect of the cells, resulting in similar confluence rate as cells treated with 0.1 % DMSO.

3.4. Tumor organoids study

DHODH has been implicated as a target in several malignancies, including colorectal cancer (Yamaguchi et al., 2019), but the involvement in primary cells from human cancer patients has not been tested. To evaluate the consequences of DHODH inhibition in colorectal cancer we studied three independent patient-derived tumor organoids (PDTO #1–3). Cell viability measurements after dose titration of IPP/CNRS-A017 showed pronounced growth inhibition in all organoids with an IC_{50} ranging from 0.1 to 0.2 μM (Fig. 6A–C). In contrast, the negative control compound IPP/CNRS-A019, showed a 50-fold decreased activity, with an IC_{50} ranging from 5.7 to 11.4 μM. Selective toxicity of A017 was confirmed by rescue in presence of 10 μg/ml uridine and the results were confirmed by morphological analysis that showed perturbed growth only in presence of IPP/CNRS-A017 alone (Fig. 6D).

4. Summary & conclusion

This study reveals the binding mode of IPP/CNRS-A017 to its target enzyme hDHODH. The inhibitor is occupying the ubiquinone binding site and therefore preventing its cofactor FMN from reoxidisation, which is ultimately leading to an inactivated protein.

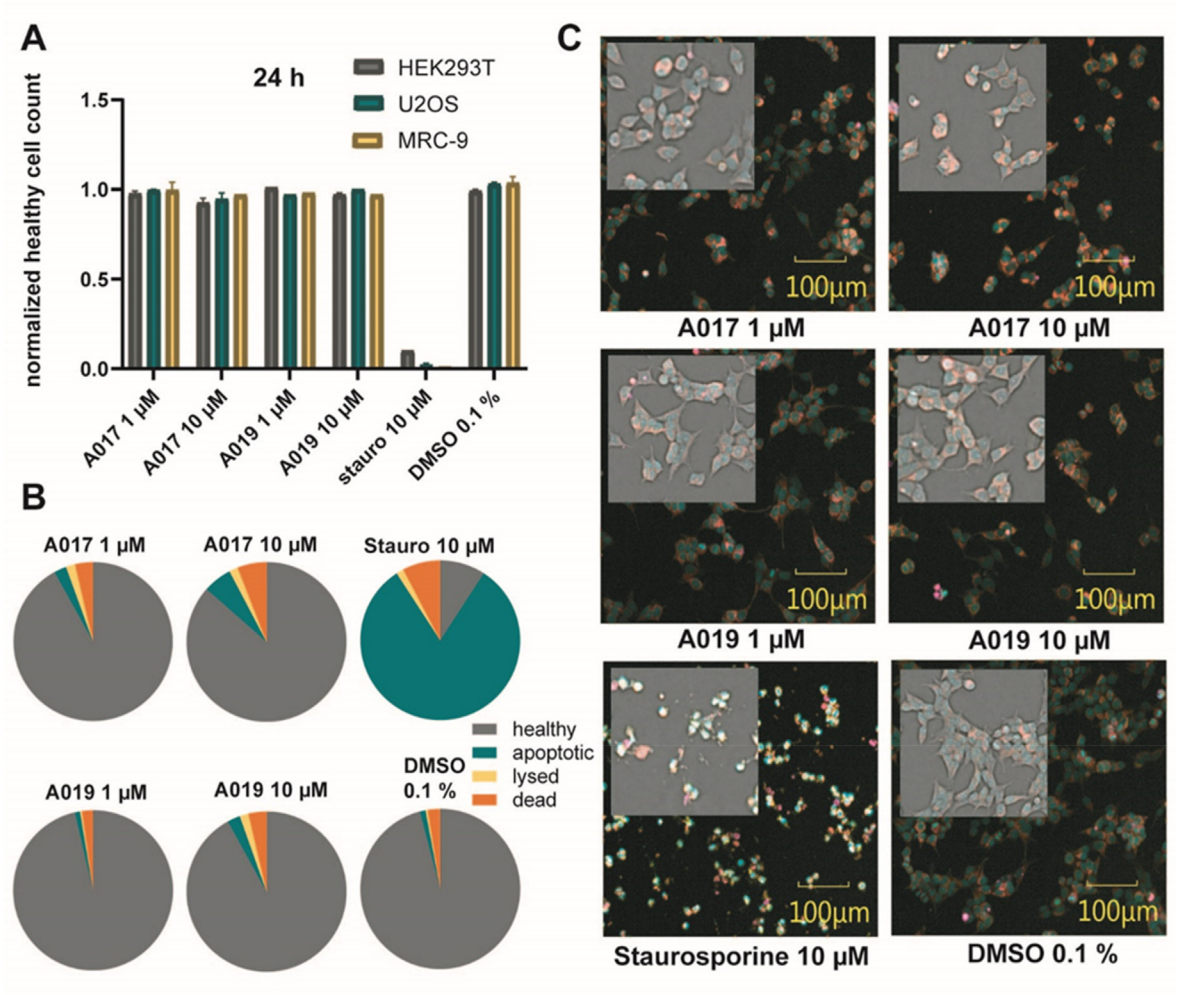

Fig. 4. Live cell high content screen of HEK293T, U2OS and MRC-9 cells. A: Healthy cell count after 24 h of 10 µM and 1 µM compound exposure (**A017**, **A019**, staurosporine (stauro)) normalized to healthy cells exposed to DMSO 0,1% in HEK293T, U2OS and MRC-9 cells. Error bars show SEM of three technical replicates. **B:** Fraction of healthy, apoptotic, lysed and dead cells after 24 h of 10 µM and 1 µM compound exposure, respectively (**A017**, **A019**, staurosporie) in comparison to 0,1% DMSO control in HEK293T cells. **C:** Fluorescence image and highlighted brightfield confocal image of stained (blue: DNA/nuclei, green: microtutubule, red: mitochondria, magenta: Annexin V apoptosis marker) HEK293T cells after 24 h of 10 µM and 1 µM compound exposure (**A017**, **A019**, staurosporine) in comparison to 0,1% DMSO control. Additional high-content data of U2OS and MRC-9 cells shown in Supplementary Fig. S1. (For interpretation of the references to color in this figure legend, the reader is referred to the Web version of this article.)

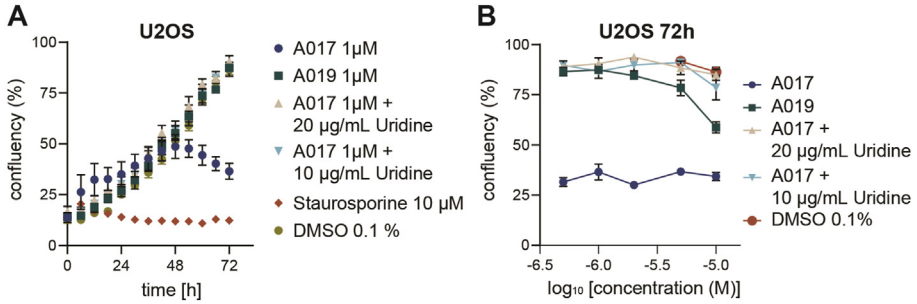

Fig. 5. Uridine rescue experiment in U2OS cells. A: Confluence (%) over 72 h at 1 µM compound exposure (**A017**, **A019)** in the presence or absence of 10 µg/mL or 20 µg/mL uridine in comparison to U2OS cells exposed to DMSO 0,1%. Error bars show SEM of four technical replicates. **B:** Confluence (%) after 72 h of a 6fold (0,5 µM, 1 µM, 2 µM, 5 µM, 10 µM) compound dilution (**A017**, **A019)** in the presence or absence of 10 µg/mL or 20 µg/mL uridine in comparison to U2OS cells exposed to DMSO 0,1%. Error bars show SEM of four technical replicates.

The well characterised IPP/CNRS-A017 and its negative control have been additionally profiled in a kinome and GPCR panel, revealing no off-targets, suggesting that the developed inhibitor is a useful chemical probe. Furthermore, a cellular quality control demonstrated no general toxicity of both compounds in three different cell lines. Study of patient-derived organoids showed a common sensitivity to IPP/CNRS-A017 but not to the negative control suggesting a specific vulnerability of colorectal cancer cells for inhibition of pyrimidine biosynthesis. Similar to the results observed for the negative control, in the performed uridine rescue experiments the effect of the probe was completely reversed.

Given the renewed interest from industrial and academic research in DHODH as a target in various diseases from viral (Lucas-Hourani et al., 2015; Munier-Lehmann et al., 2015) and parasitic infections (Madak et al., 2019) such as malaria (Phillips and Rathod, 2010), rheumatoid arthritis (Munier-Lehmann et al., 2013), autoimmune eye disease (uveitis) (Marco et al., 2018), hematologic malignancies (Sykes, 2018),

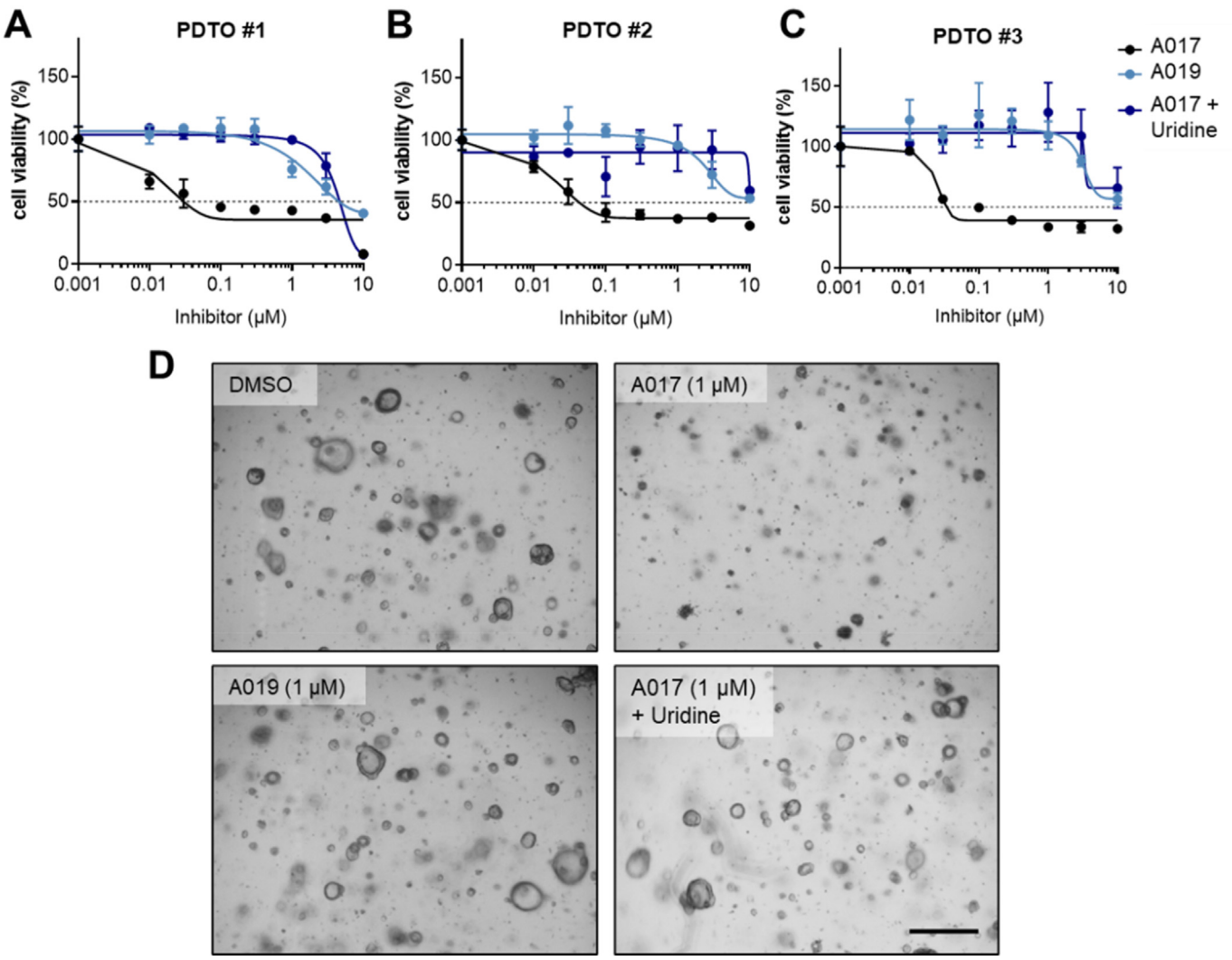

Fig. 6. IPP/CNRS-A017 shows specific toxicity in patient-derived tumor organoids. A–C: Organoids from colon cancer (PDTO #1) and rectal cancer (PDTO #2 and #3) were cultured in presence of variable concentrations of IPP/CNRS-A017 (black lines), negative control compound (IPP/CNRS-A019; light blue) or IPP/CNRS-A017 in presence of 10 μg/ml Uridine (dark blue). Cell viability was determined by CellTiter Glo assay after 4 days (mean ± SD in triplicates). D: Brightfield images of PDTO #3 after 4 days of treatment. 1 μM A017 results in marked toxicity. Organoids treated with DMSO (left), 1 μM IPP/CNRS-A019 or 1 μM IPP/CNRS-A017 in presence of uridine show unaffected morphology. Scale bar is 500 μm. (For interpretation of the references to color in this figure legend, the reader is referred to the Web version of this article.)

relapsing-remitting multiple sclerosis (RRMS) (Liu et al., 2000) and inflammatory bowel disease (Leban and Vitt, 2011) to cancers such as acute myeloid leukemia (AML) (Christian et al., 2019; Sykes et al., 2016) or diffuse large B-cell lymphoma (DLBCL) (Eheim et al., 2019), the potential application of this probe has a very broad spectrum. In a previous study we showed the effects of IPP/CNRS-A017 on measles virus replication (Lucas-Hourani et al., 2015; Munier-Lehmann et al., 2015). In the present work, we extend the analysis to show the effect of selective DHODH inhibition on three independent patient-derived tumor organoids (PDTO #1–3). The effect of the chemical probe IPP/CNRS-A-017 was specific as shown by two different control experiments, treatment with a matched negative control compound and co-treatment of IPP/CNRS-A017 with uridine, which both had no effect on growth of the tumor organoids. Our work thus extends previous work on other DHODH inhibitors and the clinical compound Brequinar that described DHODH as target for the treatment of solid cancers as well as more recently for myeloid malignancies as described for BAY 2402234 (Xiong et al., 2020; Sykes et al., 2016). Indeed, BAY 2402234 has been shown to have a dual mode of action, inhibiting proliferation of myeloid cells as well as inducing differentiation (Christian et al., 2019). Nevertheless, a recent evaluation of the effect of Brequinar in colorectal cancers showed lack of efficacy due to high DHODH levels in the tumor (Peters, 2018). Further studies will be necessary to evaluate the best system of DHODH inhibitors.

With multiple companies moving forward to clinical trials with this targeting strategy, we predict that the benefit of DHODH inhibitors will be comprehensively evaluated in the coming years. Therefore, we offer this well characterized probe and the associated data as part of the Donated Chemical Probes (DCP) library with no restriction on use (https://www.sgc-ffm.uni-frankfurt.de/).

Declaration of competing interest

The authors declare that they have no known competing financial interests or personal relationships that could have appeared to influence the work reported in this paper.

Acknowledgements

We thank Sara Stier for technical support. This work has received support from the EU/EFPIA/OICR/McGill/KTH/Diamond Innovative Medicines Initiative 2 Joint Undertaking (EUbOPEN grant n° 875510) and was supported by the LOEWE Center "Frankfurt Cancer Institute"

funded by the Hessen State Ministry for Higher Education, Research and the Arts [III L 5–519/03/03.001 - (0015)]. We also thank the lab of Marco Lucio Lolli (Turin, Italy) for kindly sharing the plasmid of hDHODH with us. A.T. is supported by the SFB 1177 'Molecular and Functional Characterization of Selective Autophagy'. The CQ1 confocal microscope (Yokogawa) was funded by: FUGG INST 161/920-1.

Appendix A. Supplementary data

Supplementary data to this article can be found online at https://doi.org/10.1016/j.crchbi.2022.100034.

References

Abt, E.R., Rosser, E.W., Durst, M.A., Lok, V., Poddar, S., Le, T.M., Cho, A., Kim, W., Wei, L., Song, J., et al., 2019. Metabolic modifier screen reveals secondary targets of protein kinase inhibitors within nucleotide metabolism. Cell Chem. Biol. 27 (2), 197–205.e6, 20 February 2020.

Arrowsmith, C.H., Audia, J.E., Austin, C., Baell, J., Bennett, J., Blagg, J., Bountra, C., Brennan, P.E., Brown, P.J., Bunnage, M.E., et al., 2015. The promise and peril of chemical probes. Nat. Chem. Biol. 11, 536–541.

Baumgartner, R., Walloschek, M., Kralik, M., Gotschlich, A., Tasler, S., Mies, J., Leban, J., 2006. Dual binding mode of a novel series of DHODH inhibitors. J. Med. Chem. 49, 1239–1247.

Besnard, J., Ruda, G.F., Setola, V., Abecassis, K., Rodriguiz, R.M., Huang, X.P., Norval, S., Sassano, M.F., Shin, A.I., Webster, L.A., et al., 2012. Automated design of ligands to polypharmacological profiles. Nature 492, 215–220.

Boschi, D., Pippione, A.C., Sainas, S., Lolli, M.L., 2019. Dihydroorotate dehydrogenase inhibitors in anti-infective drug research. Eur. J. Med. Chem. 183, 111681.

Breedveld, F.C., Dayer, J.M., 2000. Leflunomide: mode of action in the treatment of rheumatoid arthritis. Ann. Rheum. Dis. 59, 841–849.

Christian, S., Merz, C., Evans, L., Gradl, S., Seidel, H., Friberg, A., Eheim, A., Lejeune, P., Brzezinka, K., Zimmermann, K., et al., 2019. The novel dihydroorotate dehydrogenase (DHODH) inhibitor BAY 2402234 triggers differentiation and is effective in the treatment of myeloid malignancies. Leukemia 33, 2403–2415.

Drewes, G., Knapp, S., 2018. Chemoproteomics and chemical probes for target discovery. Trends Biotechnol. 36, 1275–1286.

Eheim, A., Christian, S., Meyer, H., Stoeckigt, D., Merz, C., Zimmermann, K., Bauser, M., Haegebarth, A., Ferrara, S., Sykes, D.B., et al., 2019. Abstract 3597: BAY 2402234: preclinical evaluation of a novel, selective dihydroorotate dehydrogenase (DHODH) inhibitor for the treatment of diffuse large B-cell lymphoma (DLBCL). Cancer Res. 79, 3597, 3597.

Emsley, P., Cowtan, K., 2004. Coot: model-building tools for molecular graphics. Acta Crystallogr D Biol Crystallogr 60, 2126–2132.

Evans, P.R., Murshudov, G.N., 2013. How good are my data and what is the resolution? Acta Crystallogr. Sect. D Biol. Crystallogr. 69, 1204–1214.

Fox, R.I., Herrmann, M.L., Frangou, C.G., Wahl, G.M., Morris, R.E., Strand, V., Kirschbaum, B.J., 1999. Mechanism of action for leflunomide in rheumatoid arthritis. Clin. Immunol. 93, 198–208.

Heitel, P., Faudone, G., Helmstädter, M., Schmidt, J., Kaiser, A., Tjaden, A., Schröder, M., Müller, S., Schierle, S., Pollinger, J., et al., 2020. A triple farnesoid X receptor and peroxisome proliferator-activated receptor α/δ activator reverses hepatic fibrosis in diet-induced NASH in mice. Commun. Chem. 3, 174.

Howarth, A., Schröder, M., Montenegro, R.C., Drewry, D.H., Sailem, H., Millar, V., Müller, S., Ebner, D.V., 2020. HighVia—a flexible live-cell high-content screening pipeline to assess cellular toxicity. Slas Discov.: Adv. Sci. Drug Discov. 25, 801–811.

Kabsch, W., XDS, 2010. Acta Crystallogr. Sect. D Biol. Crystallogr. 66, 125–132.

Leban, J., Vitt, D., 2011. Human dihydroorotate dehydrogenase inhibitors, a novel approach for the treatment of autoimmune and inflammatory diseases. Arzneimittelforschung 61, 66–72.

Lebedev, A.A., Vagin, A.A., Murshudov, G.N., 2008. Model preparation in MOLREP and examples of model improvement using X-ray data. Acta Crystallogr. Sect. D Biol. Crystallogr. 64, 33–39.

Liu, S., Neidhardt, E.A., Grossman, T.H., Ocain, T., Clardy, J., 2000. Structures of human dihydroorotate dehydrogenase in complex with antiproliferative agents. Structure 8, 25–33.

Lucas-Hourani, M., Munier-Lehmann, H., El Mazouni, F., Malmquist, N.A., Harpon, J., Coutant, E.P., Guillou, S., Helynck, O., Noel, A., Scherf, A., et al., 2015. Original 2-(3-alkoxy-1H-pyrazol-1-yl)azines inhibitors of human dihydroorotate dehydrogenase (DHODH). J. Med. Chem. 58, 5579–5598.

Müller, S., Ackloo, S., Arrowsmith, C.H., Bauser, M., Baryza, J.L., Blagg, J., Böttcher, J., Bountra, C., Brown, P.J., Bunnage, M.E., et al., 2018. Donated chemical probes for open science. Elife 7.

Madak, J.T., Bankhead, A., Cuthbertson, C.R., Showalter, H.D., Neamati, N., 2019. Revisiting the role of dihydroorotate dehydrogenase as a therapeutic target for cancer. Pharmacol. Therapeut. 195, 111–131.

Marco, L.L., Stefano, S., Agnese, C.P., Marta, G., Donatella, B., Franco, D., 2018. Use of human dihydroorotate dehydrogenase (hDHODH) inhibitors in autoimmune diseases and new perspectives in cancer therapy. Recent Pat. Anti-Cancer Drug Discov. 13, 86–105.

Munier-Lehmann, H., Vidalain, P.O., Tangy, F., Janin, Y.L., 2013. On dihydroorotate dehydrogenases and their inhibitors and uses. J. Med. Chem. 56, 3148–3167.

Munier-Lehmann, H., Lucas-Hourani, M., Guillou, S., Helynck, O., Zanghi, G., Noel, A., Tangy, F., Vidalain, P.O., Janin, Y.L., 2015. Original 2-(3-alkoxy-1H-pyrazol-1-yl) pyrimidine derivatives as inhibitors of human dihydroorotate dehydrogenase (DHODH). J. Med. Chem. 58, 860–877.

Peters, G.J., 2018. Re-evaluation of Brequinar sodium, a dihydroorotate dehydrogenase inhibitor. Nucleos Nucleot. Nucleic Acids 37, 666–678.

Phillips, M.A., Rathod, P.K., 2010. Plasmodium dihydroorotate dehydrogenase: a promising target for novel anti-malarial chemotherapy. Infect. Disord. - Drug Targets 10, 226–239.

Rawls, J., Knecht, W., Diekert, K., Lill, R., Löffler, M., 2000. Requirements for the mitochondrial import and localization of dihydroorotate dehydrogenase. Eur. J. Biochem. 267, 2079–2087.

Reis, R.A.G., Calil, F.A., Feliciano, P.R., Pinheiro, M.P., Nonato, M.C., 2017. The dihydroorotate dehydrogenases: past and present. Arch. Biochem. Biophys. 632, 175–191.

Sainas, S., Pippione, A.C., Giorgis, M., Lupino, E., Goyal, P., Ramondetti, C., Buccinna, B., Piccinini, M., Braga, R.C., Andrade, C.H., et al., 2017. Design, synthesis, biological evaluation and X-ray structural studies of potent human dihydroorotate dehydrogenase inhibitors based on hydroxylated azole scaffolds. Eur. J. Med. Chem. 129, 287–302.

Sykes, D.B., 2018. The emergence of dihydroorotate dehydrogenase (DHODH) as a therapeutic target in acute myeloid leukemia. Expert Opin. Ther. Targets 22, 893–898.

Sykes, D.B., Kfoury, Y.S., Mercier, F.E., Wawer, M.J., Law, J.M., Haynes, M.K., Lewis, T.A., Schajnovitz, A., Jain, E., Lee, D., et al., 2016. Inhibition of dihydroorotate dehydrogenase overcomes differentiation blockade in acute myeloid leukemia. Cell 167, 171–186 e115.

Tjaden, A., Chaikuad, A., Kowarz, E., Marschalek, R., Knapp, S., Schröder, M., Müller, S., 2022. Image Based Annotation of Chemogenomic Libraries for Phenotypic Screening. Preprints.

Vagin, A.A., Steiner, R.A., Lebedev, A.A., Potterton, L., McNicholas, S., Long, F., Murshudov, G.N., 2004. REFMAC5 dictionary: organization of prior chemical knowledge and guidelines for its use. Acta Crystallogr D Biol Crystallogr 60, 2184–2195.

van de Wetering, M., Francies, H.E., Francis, J.M., Bounova, G., Iorio, F., Pronk, A., van Houdt, W., van Gorp, J., Taylor-Weiner, A., Kester, L., et al., 2015. Prospective derivation of a living organoid biobank of colorectal cancer patients. Cell 161, 933–945.

van Riel, P.L.C.M., Smolen, J.S., Emery, P., Kalden, J.R., Dougados, M., Strand, C.V., Breedveld, F.C., 2004. Leflunomide: a manageable safety profile. J. Rheumatol. 71, 21–24.

Vyas, V.K., Ghate, M., 2011. Recent developments in the medicinal chemistry and therapeutic potential of dihydroorotate dehydrogenase (DHODH) inhibitors. Mini Rev. Med. Chem. 11, 1039–1055.

Xiong, R., Zhang, L., Li, S., Sun, Y., Ding, M., Wang, Y., Zhao, Y., Wu, Y., Shang, W., Jiang, X., et al., 2020. Novel and potent inhibitors targeting DHODH are broad-spectrum antivirals against RNA viruses including newly-emerged coronavirus SARS-CoV-2. Protein Cell 11, 723–739.

Yamaguchi, N., Weinberg, E.M., Nguyen, A., Liberti, M.V., Goodarzi, H., Janjigian, Y.Y., Paty, P.B., Saltz, L.B., Kingham, T.P., Loo, J.M., et al., 2019. PCK1 and DHODH drive colorectal cancer liver metastatic colonization and hypoxic growth by promoting nucleotide synthesis. Elife 8, e52135.